PCCP

View Online / Journal Homepage
Dynamic Article Links

Cite this: DOI: 10.1039/c2cp40519a

www.rsc.org/pccp

PAPER

Two-dimensional measurements of the solvent structural relaxation dynamics in dipolar solvation†

Sungnam Park,*[a] Jeongho Kim[b] and Norbert F. Scherer*[c]

Received 20th February 2012, Accepted 12th April 2012
DOI: 10.1039/c2cp40519a

Resonant-pump polarizability response spectroscopy (RP-PORS) is based on an optical heterodyne detected transient grating (OHD-TG) method with an additional resonant pump pulse. In RP-PORS, the resonant pump pulse excites the solute–solvent system and the subsequent relaxation of the solute–solvent system is monitored by the OHD-TG spectroscopy. RP-PORS is shown to be an excellent experimental tool to directly measure the solvent responses in solvation. In the present work, we extended our previous RP-PORS (Park *et al.*, *Phys. Chem. Chem. Phys.*, 2011, **13**, 214–223) to measure time-dependent transient solvation polarizability (TSP) spectra with Coumarin153 (C153) in acetonitrile. The time-dependent TSP spectra showed how the different solvent intermolecular modes were involved in different stages of the solvation process. Most importantly, the inertial and diffusive components of the solvent intermolecular modes in solvation were found to be spectrally and temporally well-separated. In a dipolar solvation of C153, high-frequency inertial solvent modes were found to be driven instantaneously and decay on a subpicosecond timescale while low-frequency diffusive solvent modes were induced slowly and decayed on a picosecond timescale. Our present result is the first experimental manifestation of frequency-dependent solvent intermolecular response in a dipolar solvation.

I. Introduction

Although the collective chemical intuition about the effect of solvent properties on chemical reactivity is encyclopedic,[1] our understanding of solvent dynamics during reactions is less comprehensive. This arises mainly from the difficulty of directly measuring the solvent in reactions and interpretation of the complex responses.[2–4] The fundamental aspects of solvent dynamics in reactions can be studied by a simpler solvation process.[5] As schematically depicted in Fig. 1(A), solvation is a relaxation process of a solute–solvent system after a sudden perturbation of the electronic structure of the solute.[5–8] Following electronic excitation of the solute, the solvent molecules surrounding the solute undergo the time-dependent structural reorganization.[5,9–11] The solvent molecules reorganize *via* translational and orientational motions to achieve a new equilibrium solute–solvent configuration.

Solvation dynamics have been extensively investigated by time-resolved fluorescence Stokes shift (TRFSS)[12–14] and photon echo peak shift (PEPS)[10,15–18] measurements. The major finding from TRFSS and PEPS is that the solvation occurs in a bimodal fashion, exhibiting the fast inertial and relatively slow diffusive motions of the solvent.[5,6,19] The ultrafast inertial component plays important roles in the early stage of the solvation while the diffusive motion is responsible for solvation at longer times and is well described by exponential functions.[6,8,10,20,21] In addition, the relative contribution of the inertial and diffusive motions is solvent-dependent. For example, the ultrafast inertial component in acetonitrile and water is dominant (nearly 70–80% of the total solvation decay) whereas that in methanol and formamide accounts for only 30–40%. The diffusive motion plays more important roles in weakly polar and non-dipolar solvents such as chloroform and benzene, respectively.[8,13] In fact, the quantities measured in TRFSS and PEPS provide indirect information on *what the solvent is actually doing* because the solute's spectroscopic properties associated with the solvent relaxation or fluctuation are measured using both experimental methods. However, although a direct measurement of the solvent responses in solvation is required to get more detailed information, it is quite experimentally challenging.[3,22–27]

To directly measure the solvent intermolecular responses in solvation, we developed the resonant-pump polarizability response spectroscopy (RP-PORS).[4,25] RP-PORS is based on the optical heterodyne detected transient grating (OHD-TG) spectroscopy with an additional excitation pump beam as

[a] *Department of Chemistry, Korea University, Seoul, 136-701, Korea. E-mail: spark8@korea.ac.kr*
[b] *Department of Chemistry, KAIST, Yuseong-gu, Daejeon, 305-701, Korea*
[c] *Department of Chemistry, the Institute for Biophysical Dynamics and the James Franck Institute, University of Chicago, Chicago, Illinois 60637, USA. E-mail: nfschere@uchicago.edu*
† Electronic supplementary information (ESI) available. See DOI: 10.1039/c2cp40519a

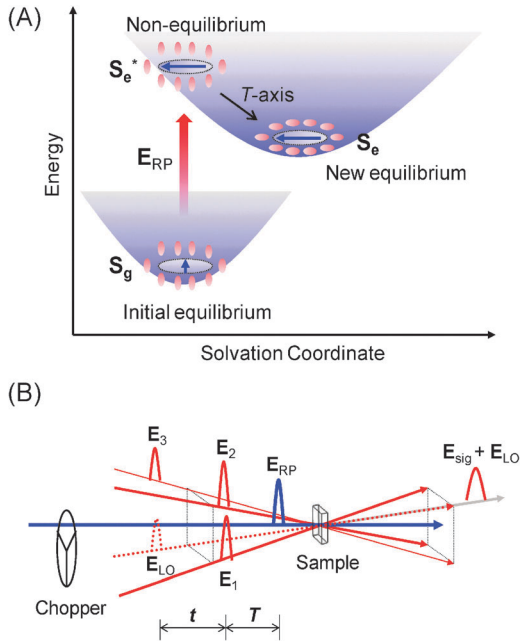

Fig. 1 (A) Schematic illustration of the solvation dynamics. S_g represents an initial equilibrium state between the ground state solute and solvents while S_e represents a new equilibrium state between the excited state solute and solvents. S_e^* is a nonequilibrium state created by an electronic excitation of the solute. (B) Definition of time variables (T and t), pulse sequence, and beam geometry in resonant-pump polarizability response spectroscopy (RP-PORS). See ref. 4 for more details.

shown in Fig. 1(B). Recently, the detailed theoretical description and simulation for the RP-PORS were also presented.[27] The RP-PORS is theoretically considered as a fifth-order spectroscopy where the resonant pulse created the ground (hole) and excited-state (particle) wavepackets that evolve until the polarizability spectrum is probed by three incident nonresonant pulses and a fourth local oscillator pulse.[4,27] The model simulation showed that the PORS signal generation could result from (1) the structural relaxation induced resonance and (2) the dephasing induced resonance.[27] The lineshapes obtained from both the model simulation based on two mechanisms and the RP-PORS experiments had suggested that the structural relaxation induced resonance was more important than the dephasing induced resonance.[27] RP-PORS was shown to be an excellent experimental method for directly measuring the solvent relaxation dynamics in solvation.[4] As shown in Fig. 1(B), there are two time variables (T and t) in RP-PORS. The equilibrium solute–solvent state is perturbed by the electronic excitation of the solute from S_g to S_e^* in Fig. 1(A) with an ultrashort resonant pulse ($\boldsymbol{E}_{RP}$) at $T = 0$ ps. After a delay time of T, the solvent structural changes are measured by OHD-TG spectroscopy.[4] By controlling the phase of the local oscillator with respect to the signal in RP-PORS, the dispersive part of the OHD-TG signal is selectively measured and is termed "polarizability response". For the remainder of our present paper, polarizability response spectroscopy (PORS) means the OHD-TG spectroscopy measuring the dispersive part of the signal. If T is larger than T_{eq} (the complete solvation time, *i.e.* the time for completion of solvent relaxation), PORS measures the difference in equilibrium solvent structure or fluctuation around the solute in S_g and S_e. If T is smaller than T_{eq}, PORS measures non-equilibrium solvent relaxation around the solute.

In the present paper, we extended our previous RP-PORS (Park *et al.*, *Phys. Chem. Chem. Phys.*, 2011, **13**, 214–223) into a two-dimension by scanning both t-axis and T-axis, which is termed "two-dimensional polarizability response spectroscopy (2D-PORS)". The PORS signal measured at a fixed $T > T_{eq}$ gives the overall solvation polarizability spectrum in solvation (*i.e.* 1D-PORS). In 2D-PORS, the time-dependent transient solvation polarizability spectra are measured in two-dimensional frequency-time axes as the solvation proceeds. 2D-PORS was performed with Coumarin153 (C153) in acetonitrile, which has been extensively used as a model system for the dipolar solvation studies.[4,13,14,20,21,25,28] Upon electronic excitation of C153, the polarizability of C153 increases by 50% and its dipole moment is raised by 7–8 Debye. Transient solvation polarizability (TSP) spectra of acetonitrile around C153 were obtained as a function of T following the electronic excitation of C153. Our 2D-PORS results showed that higher-frequency solvent intermolecular motions are induced instantaneously and decay rapidly while lower-frequency solvent intermolecular motions are slowly driven and decay slowly. In this case, high-frequency solvent intermolecular modes correspond to the initial inertial responses of the solvent while the low-frequency solvent intermolecular modes correspond to the diffusive responses of the solvent and are responsible for the solvation at long times. In addition, it was clearly observed that the inertial and diffusive components are frequency-dependent as well as temporally well-separated.

II. Experimental

An experimental method of RP-PORS was described in a great detail elsewhere.[4] In brief, a home-built cavity-dumped Ti:Sapphire oscillator and amplifier system produces 1.5 μJ pulses centered at 800 nm at repetition rates ranging from 10 to 250 kHz.[29–31] The 400 nm second harmonic pulse, which is used as a resonant pump in RP-PORS, is generated in a 200 μm thick BBO crystal. Both 800 and 400 nm pulses are properly precompensated for material dispersion with two separate pairs of BK7 prisms giving 35 fs duration pulse at 800 nm and 70 fs pulse at 400 nm sample position. An experimental setup of RP-PORS is based on an optical heterodyne detected transient grating (OHD-TG) spectrometer which is built with a diffractive optical element (DOE).[4,32–35] In the OHD-TG spectrometer, the 800 nm beam is split into two beams in a 3 : 1 intensity ratio and their relative time delay is controlled before the DOE. Two beams, which are vertically-polarized, are focused onto the DOE with an achromatic lens (f.l. = 15 cm). The DOE is specially designed and manufactured such that the total diffraction efficiency for the first-order (±1) beams is more than 80% at 800 nm (HoloEye Photonics AG, Germany). The first-order (±1) diffraction beams, whose angle is 10°, are used for the experiments. Four beams ($\boldsymbol{E}_1$, $\boldsymbol{E}_2$, $\boldsymbol{E}_3$, and $\boldsymbol{E}_{LO}$) generated from the DOE are collimated and focused onto the sample with parabolic mirrors (f.l. = 20 cm and f.l. = 15 cm, respectively) in a box-car geometry as shown in Fig. 1(B). The second-harmonic pulse (resonant pump, $\boldsymbol{E}_{RP}$), generated in a 0.2 mm thick BBO crystal, is directed towards the center of the square. The spot sizes of the 800 nm beams are ~50 μm in diameter. The pulse energies of $\boldsymbol{E}_1$, $\boldsymbol{E}_2$, $\boldsymbol{E}_3$, and $\boldsymbol{E}_{LO}$ are

approximately 30, 30, 10, and 0.5 nJ per pulse at the sample position, respectively. The spot size of the 400 nm beam is about ~75 μm in diameter and the pulse energy is about 50 nJ per pulse. The diagram of the pulse sequence and definition of time variables are shown in Fig. 1(B). The 2D-PORS signal, $S(T,t)$, is collected by selectively measuring the dispersive part of the OHD-TG signal as a function of t at successive delay times (T) after the sample is excited by the resonant-pump ($\boldsymbol{E}_{RP}$) at $T = 0$ ps. The resonant pump ($\boldsymbol{E}_{RP}$) and nonresonant pump ($\boldsymbol{E}_1$ and $\boldsymbol{E}_2$) pulses are vertically polarized. The probe ($\boldsymbol{E}_3$) and local oscillator ($\boldsymbol{E}_{LO}$) pulses are rotated by 45° with respect to the pump pulses ($\boldsymbol{E}_{RP}/\boldsymbol{E}_1/\boldsymbol{E}_2/\boldsymbol{E}_3/\boldsymbol{E}_{LO}$ = 0°/0°/0°/45°/45°). The vertical and horizontal components of the OHD-TG signal are decomposed before the detection by a Rochon polarizer and are measured simultaneously (see Fig. S1 in the ESI†).[4] In RP-PORS, a resonant pump pulse, $\boldsymbol{E}_{RP}(\boldsymbol{k}_{RP})$, excites a chromophore (*i.e.* C153) at $T = 0$ ps. At a time delay, T, the two nonresonant pump pulses, $\boldsymbol{E}_1(\boldsymbol{k}_1)$ and $\boldsymbol{E}_2(\boldsymbol{k}_2)$, are temporally and spatially overlapped leading to a modulation of the complex index of refraction of the sample. At a time delay, $T + t$, the probe, $\boldsymbol{E}_3(\boldsymbol{k}_3)$, stimulates the emission of the signal, $\boldsymbol{E}_{sig}(\boldsymbol{k}_{sig} = -\boldsymbol{k}_1 + \boldsymbol{k}_2 + \boldsymbol{k}_3)$, to a new phase matched direction. The emitted signal field is interferometrically mixed with the local oscillator (LO) allowing the optical heterodyne detection. In our experimental geometry, the LO, $\boldsymbol{E}_{LO}(\boldsymbol{k}_{LO})$, is also overlapped with other incoming pulses ($\boldsymbol{E}_n(\boldsymbol{k}_n) = \boldsymbol{E}_{RP}(\boldsymbol{k}_{RP})$, $\boldsymbol{E}_1(\boldsymbol{k}_1)$, $\boldsymbol{E}_2(\boldsymbol{k}_2)$, and $\boldsymbol{E}_3(\boldsymbol{k}_3)$) in the sample and the degenerate pump–probe signals ($\boldsymbol{E}'_{sig}(\boldsymbol{k}'_{sig})$) in the same phase-matched direction ($\boldsymbol{k}'_{sig} = -\boldsymbol{k}_n + \boldsymbol{k}_n + \boldsymbol{k}_{LO}$) are also measured together with the OHD-TG signal ($\boldsymbol{k}_{sig} = \boldsymbol{k}'_{sig}$). However, the degenerate pump–probe signals are always in-phase with the LO while the OHD-TG signal is dependent upon the phase of the LO. Therefore, the dispersive part of the OHD-TG signal at a given T can be obtained by a dual phase scan method

$$S_{disp}(t;T) = S(t,\phi = \pi/2;T) - S(t,\phi = 3\pi/2;T) \propto \mathrm{Re}[P^{(3)}(t;T)] \quad (1)$$

In practice, the RP-PORS signals are obtained by measuring the OHD-TG signals with two π/2 out-of-phase local oscillators and taking their difference.[4] The RP-PORS signals are superimposed on top of the degenerate pump–probe signals (see Fig. S2 in the ESI†). These degenerate pump–probe signals ($\boldsymbol{E}_{RP}$ and $\boldsymbol{E}_{LO}$) are a time-dependent background. However, they are independent of the phase of the LO and thus can be removed by the dual phase scan method.

Sample C153 purchased from Acros was used as received. Acetonitrile used in the experiments was of HPLC-grade. 0.30 mM C153 solution was prepared by directly dissolving C153 in acetonitrile. The C153 solution sample was circulated in a flow-through cell with 1 mm pathlength during the measurement to avoid photobleaching and thermal heating. The repetition rate of pulses from the laser system was 123 kHz so that the time interval between pulses in a train of pulses is 8 μs ensuring that C153, whose lifetime in the excited state is ~5 ns, relaxes back to the ground state before the next pulse arrives. Two sets of identical detector and lock-in amplifier are used to measure both S_{zzzz} and S_{yyzz} signals at the same time by chopping the resonant pump at 2.51 kHz.[4]

It should be mentioned that the signals are collected in RP-PORS by chopping the resonant pump ($\boldsymbol{E}_{RP}$). Therefore, the measured RP-PORS signal can be written as

$$S(t;T) = S_{RP\text{-}On}(t;T) - S_{RP\text{-}Off}(t;T) \quad (2)$$

where $S_{RP\text{-}On}(t;T)$ and $S_{RP\text{-}Off}(t;T)$ represent the molecular responses with the resonant pump on and off, respectively. The resonant pump is resonant only with the solute (*i.e.* C153) and nonresonant with the solvent. Therefore, the RP-PORS measures only the molecular responses that are influenced by the electronic excitation of the solute. This allows a selectivity of the molecular responses that are induced *only* by the resonant pump. Thus, the solvent molecular response in bulk is not measured in RP-PORS.

III. Results and data analysis

The 2D-PORS signal, $S(T,t)$, is collected by scanning t at a series of T. T is a waiting time before the PORS measurement is performed as shown in Fig. 1(B). In this particular case, the T-axis is thought of as "the solvation axis". As mentioned in Introduction, the 2D-PORS signal results from the solvent structural relaxation that is achieved mainly by the translational and orientational motions of the solvent molecules around the solute following the electronic excitation of the solute. Furthermore, the solvent structural relaxations can be separated into the isotropic and anisotropic responses based on their symmetry.[36–38] The isotropic and anisotropic PORS signals are obtained by,[4,39]

$$S_{iso}(T,t) = \frac{1}{3}[S_{zzzz}(T,t) + 2S_{yyzz}(T,t)] \quad (3)$$

$$S_{aniso}(T,t) = \frac{1}{2}[S_{zzzz}(T,t) - S_{yyzz}(T,t)] \quad (4)$$

where $S_{zzzz}(T,t)$ and $S_{yyzz}(T,t)$ represent polarizability tensor elements that are parallel and perpendicular to the solute transition dipole, respectively. Fig. 2 displays the isotropic and anisotropic 2D-PORS signals measured with C153 in acetonitrile. The isotropic response, $S_{iso}(T,t)$, is sensitive to isotropic solvent reorganization (*i.e.* isotropic change in solvent local density) around the solute caused by isotropic (centrosymmetric) molecular translational motions. On the other hand, the anisotropic response, $S_{aniso}(T,t)$, selectively measures anisotropic solvent reorganization around the solute caused by anisotropic (non-centrosymmetric) molecular translational motions and molecular orientations.[4] The PORS signal measured at a given T can be written as a convolution of the polarizability response function, $R(T,t)$, and the instrumental response function, $G(t)$,[40]

$$S(t;T) = \int \mathrm{d}\tau G(\tau) R(\tau - t;T) \quad (5)$$

$$R(t;T) = R^{el}(t;T) + R^{nuc}(t;T) \quad (6)$$

where $R(t;T)$ can be written as the sum of the electronic response function, $R^{el}(t;T)$, and the nuclear response function, $R^{nuc}(t;T)$, within the Born–Oppenheimer approximation. The nuclear response function, $R^{nuc}(t;T)$, includes all nuclear dynamics that are observed in the PORS. The nuclear response

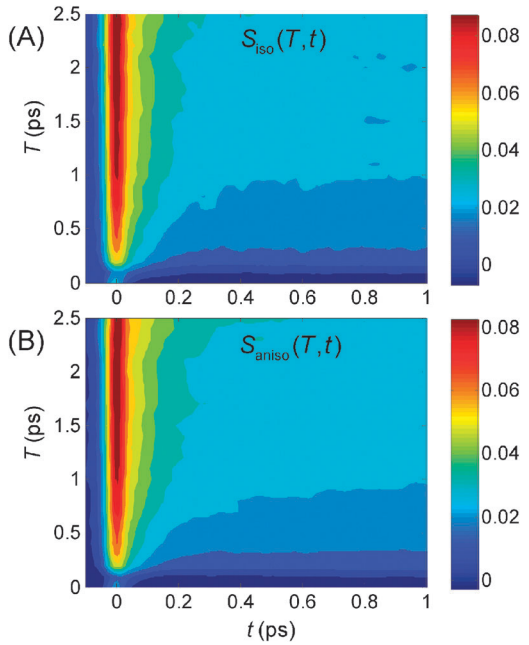

Fig. 2 Isotropic and anisotropic 2D-PORS signals measured with C153 in acetonitrile. The t-scan is made by varying T. The T-axis represents the solvation axis. The solvation is almost finished at $T = 2.5$ ps. The t-axis is shown up to $t = 1.0$ ps.

function can be further separated into two contributions at a given T[4,25]

$$R^{nuc}(t;T) = R'(t;T) + R^{solute}(t;T) \quad (7)$$

where $R^{solute}(t;T)$ represents the long time component observed in the PORS signal and $R'(t;T)$ describes all nuclear dynamics occurring on a shorter timescale than $R^{solute}(t;T)$. The isotropic and anisotropic responses contain different longer time solute contributions.[4] In order to focus more on the solvent relaxation dynamics on a shorter timescale, the longer time contributions, $R^{solute}(t;T)$, are convoluted with the instrumental response function and are removed from the PORS signal at a given T,[4,25]

$$\begin{aligned} S'(t;T) &= S(t;T) - \int d\tau G(\tau)H(\tau - t)R^{solute}(\tau - t;T) \\ &= \int d\tau G(\tau)R'(\tau - t;T) \end{aligned} \quad (8)$$

where $H(t)$ is the Heaviside step function and $R^{solute}(t;T)$ is a constant in the isotropic PORS signal resulting from the isotropic density change around the solute and a single exponential function in the anisotropic PORS signal arising from the reorientational motion of the solute.[4,25]

The polarizability spectrum at a given T is obtained by the Fourier deconvolution method,

$$D(\omega_t;T) = \frac{FT[S'(t;T)]}{FT[G(t)]} = FT[R'(t;T)] \quad (9)$$

where FT[$\cdots$] denotes the Fourier transformation and $D(\omega_t;T) = Re[D(\omega_t;T)] + iIm[D(\omega_t;T)]$. $\chi(\omega_t;T) = Im[D(\omega_t;T)]$ denotes the polarizability spectrum of solvation and captures all nuclear motions that are present in $R'(t;T)$.

$\chi(\omega_t;T)$ is the 2D frequency–time data that are directly obtained from the Fourier transformation. To interpret $\chi(\omega_t;T)$ properly, information contents in $\chi(\omega_t;T)$ need to be discussed by taking into account the experimental scheme in Fig. 1(B) and underlying dynamics. In 2D-PORS, the solvent structural reorganization is driven at $T = 0$ ps and T is the waiting time before the PORS signal is measured. Accordingly, the PORS signal only includes the solvent structural relaxation around C153 after a delay time of T. In other words, the solvent structural relaxation during T is not measured in the PORS signal. As T is increased, the PORS signal includes less information on the solvent structural relaxation along the solvation axis. With this idea in mind, the difference solvation polarizability spectrum along the solvation axis is calculated as

$$\Delta\chi(\omega_t;T') = \chi(\omega_t;T + \Delta T) - \chi(\omega_t;T) \quad (10)$$

where $T' = T + \Delta T/2$ and ΔT is the time interval. $\Delta\chi(\omega_t;T')$, which is termed "transient solvation polarizability (TSP) spectrum" at the solvation time of T', represents a change in the polarizability spectrum of the solvent when the solvation proceeds from T to $T + \Delta T$. In the case of C153 in acetonitrile, $\Delta\chi(\omega_t;T')$ is obtained by setting $\Delta T = 0.1$ ps, which is the minimum time step of the T-axis in our present experiment. In our current notation, $\Delta\chi(\omega_t;T' = 0.05$ ps) represents the TSP spectrum at $T' = 0.05$ ps meaning the change in the solvent intermolecular response from $T = 0$ ps to $T = 0.1$ ps during the solvation. Fig. 3 displays $\Delta\chi_{iso}(\omega_t;T')$ and $\Delta\chi_{aniso}(\omega_t;T')$ obtained with C153 in acetonitrile.

IV. Discussion

A. Transient solvation polarizability (TSP) spectra

As mentioned earlier, the isotropic and anisotropic solvation responses result from different types of solvent structural reorganization around the solute and can be separately measured in our 2D-PORS experiments. $\Delta\chi_{iso}(\omega_t;T')$ displays the time evolution of the totally symmetric (isotropic) solvent responses that lead to the isotropic change in the solvent structure around C153. On the other hand, $\Delta\chi_{aniso}(\omega_t;T')$ includes the time evolution of anisotropic solvent responses resulting from the orientational motions and anisotropic translational motions of the solvent molecules.[4] Even though the origins of both isotropic and anisotropic solvent responses are quite different, $\Delta\chi_{iso}(\omega_t;T')$ and $\Delta\chi_{aniso}(\omega_t;T')$ display similar spectral features in Fig. 3. One characteristic feature in both $\Delta\chi_{iso}(\omega_t;T')$ and $\Delta\chi_{aniso}(\omega_t;T')$ is that the maximum of the TSP spectrum is shifted to the lower frequency as T' is increased. Broad and relatively high-frequency solvent intermolecular motions are instantaneously driven right after the electronic excitation of C153. As T' is increased, the higher-frequency modes decay rapidly and the lower-frequency modes are slowly driven. It appears in Fig. 3 that the relaxation of higher-frequency modes induces the lower-frequency modes in a sequential manner. This is seen as a time lag between frequency-dependent solvent intermolecular motions in the solvation process.

To examine a few main features in more detail, the anisotropic TSP spectra at four delay times of T' are shown in Fig. 4(A).

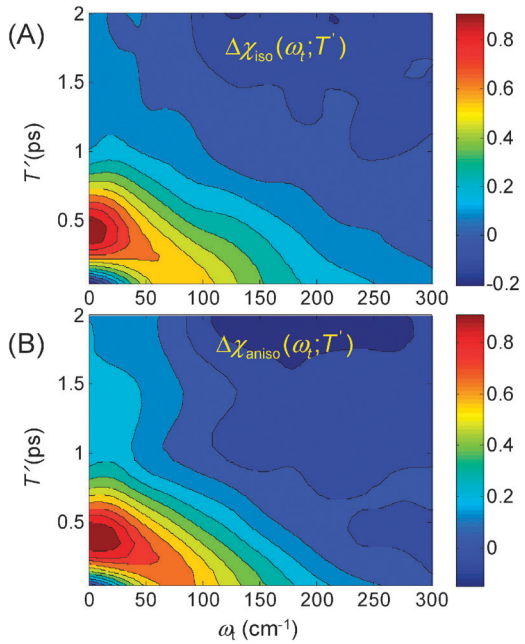

Fig. 3 (A) Isotropic and (B) anisotropic transient solvation polarizability (TSP) spectra along the solvation axis (T'-axis). Two TSP spectra are normalized by their peak maximum. General spectral features are quite similar. See the text for more details.

The anisotropic TSP spectrum at $T' = 0.05$ ps, which represents a change in the polarizability spectra of acetonitrile between $T = 0$ ps and $T = 0.1$ ps along the solvation axis, is peaked at $\sim$80 cm^{-1} and its band width is $\sim$140 cm^{-1}. At $T' = 0.45$ ps, the maximum peak of the anisotropic TSP spectrum is at $\sim$6 cm^{-1} and the band width is 80 cm^{-1}. As T' is increased from 0.05 to 0.45 ps, the maximum peak position of the anisotropic TSP spectrum is gradually shifted to the lower-frequency and the bandwidth becomes narrower. At longer times than $T' = 0.45$ ps, the maximum peak positions are not significantly changed.

As a theoretical effort to understand the solvation dynamics in polar solvents, the instantaneous normal mode (INM) analysis was used.[41–43] In the INM analysis, the displacement of the solute–solvent configuration at any time from its initial configuration can be decomposed into a set of independent and collective modes that are driven under their own harmonic potentials. It is assumed that the solvation dynamics at short times are governed by these instantaneous normal modes of the solvent. Therefore, the INM solvation spectrum is believed to be a reasonable representation of the solvent molecular modes driven during solvation at short times. It is interesting to compare our experimentally obtained TSP spectrum at a short time with the result of the instantaneous normal mode (INM) analysis. In Fig. 5, an anisotropic TSP spectrum at $T' = 0.05$ ps is compared with the INM solvation spectrum of acetonitrile, which was obtained by the INM analysis with a dipolar solute in acetonitrile.[42] Our experimentally obtained TSP spectrum at $T' = 0.05$ ps is in good agreement with the theoretically predicted INM spectrum.

Fig. 4(B) shows the time evolution of the solvent intermolecular modes at different frequencies. The solvent intermolecular mode at $\omega_t = 10$ cm^{-1} is driven slowly relative to higher-frequency modes and is peaked at $T' = 0.35$ ps. Subsequently, it decays to

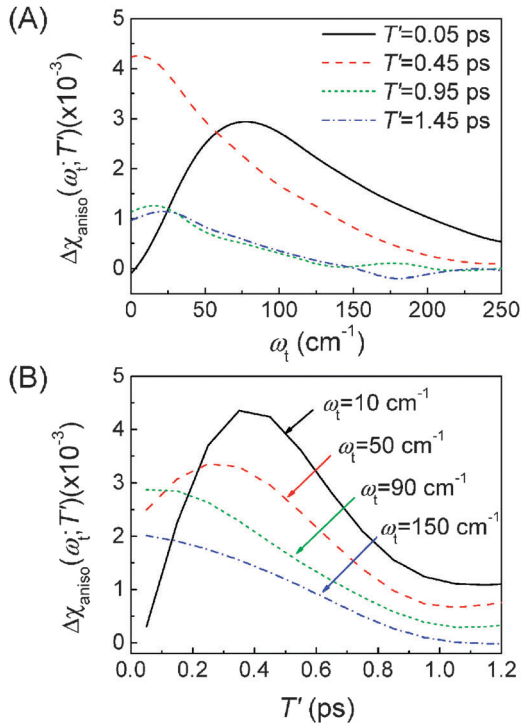

Fig. 4 Time and frequency slices of anisotropic TSP spectrum. (A) Temporal evolution of anisotropic TSP spectra as a function of T' along the solvation axis. (B) Temporal behaviors of frequency-dependent solvent intermolecular modes.

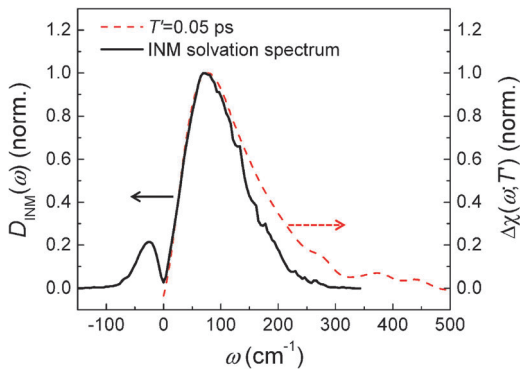

Fig. 5 Anisotropic TSP spectrum at $T' = 0.05$ ps is compared with the INM solvation spectrum. INM solvation spectrum is adapted from ref. 42.

about 25% of its maximum value in $\sim$1 ps followed by a slower decay. As the frequency of the solvent intermolecular mode is increased, the maximum point moves relatively to a shorter time in Fig. 4(B). The high-frequency solvent intermolecular mode at $\omega_t = 150$ cm^{-1} is found to be instantaneously driven and decay to zero on a subpicosecond timescale.

In short, broad and higher-frequency solvent intermolecular modes, which are associated with the fast inertial components, are responsible for the early stages of solvation and decay on a subpicosecond time scale. On the other hand, the lower-frequency modes, which are diffusive in nature, are driven relatively slowly and play an important role in solvation at longer times. In 2D-PORS, the inertial and diffusive components of the solvent in solvation are able to be spectrally distinguished as well as are temporally separated.

B. Frequency-dependent solvent intermolecular modes in dipolar solvation

Our main experimental observations are summarized as follows: (1) time-dependent isotropic and anisotropic TSP spectra are very similar, (2) high-frequency modes in the TSP spectrum are instantaneously driven and are responsible mainly for the early stages of solvation, (3) low-frequency modes are relatively slowly induced and contribute to the solvation processes at long times, and (4) there is a time lag of the solvent intermolecular motions in the solvation process. In other words, all solvent intermolecular motions are not driven at the same time in solvation but the higher-frequency solvent intermolecular motions are driven earlier than the lower-frequency solvent intermolecular motions. The time lag of the solvent intermolecular motions driven in solvation is an interesting observation in providing further mechanistic understanding of the dipolar solvation of C153. The solvation proceeds in a sequential manner. Following an electronic excitation of C153, the solvent reorganization in the first solvation shell would be achieved by higher-frequency translational and orientational motions of the solvent driven by a sudden change in the intermolecular force between the excited C153 and acetonitrile. Subsequently, the solvent reorganization in the first solvation shell would induce the solvent motions in the second solvation shell. In this case, the decay of the solvent intermolecular motions in the first solvation shell and the induction of the solvent intermolecular motions in the second solvation shell might occur at the same time. The solvent intermolecular motions in the second solvation shell would be at lower frequencies because the driving force is primarily the intermolecular potential between acetonitrile molecules in the first and second solvation shells. The solvent intermolecular motions in the second solvation shell would induce the solvent intermolecular motions in the next solvation shells. This propagation of solvent intermolecular motions would go on and on until the solvent reorganization is finished. The solvent structural reorganization in outer solvation shells might be less important in the overall solvation process but its contribution to the solvation response might not be negligibly small because the larger numbers of the solvent molecules are involved.

Before we close this section, it should be pointed out that the solvation response of acetonitrile molecules around C153 measured in RP-PORS is a lot larger than what is estimated based on the number of acetonitrile molecules around the excited C153. As mentioned earlier, the RP-PORS signal is contributed by the solvent molecules around the excited C153 because the solvent reorganization induced by the resonant excitation of C153 is measured by chopping the resonant pump beam (400 nm). The relative magnitude of the solvation response around the excited C153 to the solvent response in bulk was found to be 0.72% when we compared the PORS signals measured with C153 in acetonitrile and neat acetonitrile under the same experimental conditions (see Fig. S4 in the ESI† for more details). Based on our experimental conditions, we can estimate the number of the solvent molecules around C153 that contribute to the RP-PORS signal. The sample solution contains ~19 M acetonitrile and 0.3 mM C153. If it is assumed that there are approximately 40–50 acetonitrile molecules per C153 including the first and second solvation shells, the total concentration of acetonitrile molecules around C153 in the sample solution is ~12–15 mM. If it is further assumed that ~10% of C153 molecules are excited by the resonant pump beam and the PORS signal is proportional to the number of acetonitrile molecules around the excited C153 in the interaction volume of the sample, the magnitude of the solvation response around the excited C153 is estimated to be ~0.007% that of the bulk solvent response, which is ~100 times smaller than the experimentally measured solvation signal. The same huge enhancement of the solvation signals was also observed with C153 in different solvents (see Fig. S3 in the ESI†).

V. Summary and concluding remarks

RP-PORS was performed with C153 in acetonitrile to directly measure the transient solvation polarizability (TSP) spectra as a function of the solvation time. In contrast to TRFSS and PEPS, our experimental approach allowed the measurements of frequency-dependent solvent intermolecular motions in solvation and thus it provided more detailed information on the solvent molecular responses in solvation by directly looking at the solvent. Isotropic and anisotropic TSP spectra were able to be separately obtained by controlling the polarizations of incident beams. The TSP spectra during solvation have a bimodal character, which agrees well with the results that were previously obtained from one-dimensional experiments (*i.e.* TRFSS and PEPS). Moreover, the inertial and diffusive components, which were two major components in the bimodal solvation processes, were able to be frequency-resolved in the time-dependent TSP spectra. We found that higher-frequency solvent intermolecular motions are driven instantaneously and decay rapidly on a subpicosecond timescale whereas lower-frequency solvent intermolecular motions are induced slowly and decay on a picosecond timescale. In addition, it was also found that higher-frequency solvent motions are driven earlier than lower-frequency solvent motions such that different frequency solvent intermolecular modes participate in different stages of the solvation process.

Our present results are the first experimental manifestation of frequency-dependent inertial and diffusive solvent intermolecular motions in solvation that are also separable in time. These results imply that the solvent reorganization around the solute occurs in a sequential manner. We believe that our present 2D-PORS results reveal general features of the frequency-dependent solvent intermolecular responses in dipolar solvation. In addition, 2D-PORS can be applicable to study other non-equilibrium dynamics in solutions.

Acknowledgements

We thank Prof. Ladanyi for providing us the INM results. This research was supported by National Science Foundation (CHE0317009). This work was also supported by the NRF grant (No. 2010-0005020 and No. 2011-0002122), the Human Resources Development of the KETEP grant (No. 20104010100640) to SP.

References

1 C. Reichardt, *Solvents and Solvent Effects in Organic Chemistry*, VCH, New York, 1990.
2 C. Ryu and R. M. Stratt, *J. Phys. Chem. B*, 2004, **108**, 6782–6795.
3 D. F. Underwood and D. A. Blank, *J. Phys. Chem. A*, 2005, **109**, 3295–3306.
4 S. Park, J. Kim, A. M. Moran and N. F. Scherer, *Phys. Chem. Chem. Phys.*, 2011, **13**, 214–223.
5 R. M. Stratt and M. Maroncelli, *J. Phys. Chem.*, 1996, **100**, 12981–12996.
6 B. Bagchi and R. Biswas, *Adv. Chem. Phys.*, 1999, **109**, 207–433.
7 P. F. Barbara and W. Jarzeba, *Adv. Photochem.*, 1990, **15**, 1–68.
8 E. W. Castner and M. Maroncelli, *J. Mol. Liq.*, 1998, **77**, 1–36.
9 B. Bagchi, D. W. Oxtoby and G. R. Fleming, *Chem. Phys.*, 1984, **86**, 257–267.
10 G. R. Fleming and M. Cho, *Annu. Rev. Phys. Chem.*, 1996, **47**, 109–134.
11 B. Bagchi and B. Jana, *Chem. Soc. Rev.*, 2010, **39**, 1936–1954.
12 M. A. Kahlow, W. Jarzeba, T. J. Kang and P. F. Barbara, *J. Chem. Phys.*, 1989, **90**, 151–158.
13 M. L. Horng, J. A. Gardecki and M. Maroncelli, *J. Phys. Chem.*, 1995, **99**, 17311–17337.
14 L. Reynolds, J. A. Gardecki, S. J. V. Frankland, M. L. Horng and M. Maroncelli, *J. Phys. Chem.*, 1996, **100**, 10337–10354.
15 T. Joo, Y. Jia, J.-Y. Yu, M. J. Lang and G. R. Fleming, *J. Chem. Phys.*, 1996, **104**, 6098–6108.
16 W. P. de Boeij, M. S. Pshenichnikov and D. A. Wiersma, *Annu. Rev. Phys. Chem.*, 1998, **49**, 99–123.
17 C. J. Bardeen, S. J. Rosenthal and C. V. Shank, *J. Phys. Chem. A*, 1999, **103**, 10506–10516.
18 D. S. Larsen, K. Ohta and G. R. Fleming, *J. Chem. Phys.*, 1999, **111**, 8970–8979.
19 P. V. Kumar and M. Maroncelli, *J. Chem. Phys.*, 1995, **103**, 3038–3060.
20 H. K. Kashyap, T. Pradhan and R. Biswas, *J. Chem. Phys.*, 2006, **125**, 174506.
21 H. K. Kashyap and R. Biswas, *J. Phys. Chem. B*, 2008, **112**, 12431–12438.
22 G. Haran, W.-D. Sun, K. Wynne and R. M. Hochstrasser, *Chem. Phys. Lett.*, 1997, **274**, 365–371.
23 B. N. Flanders, D. C. Arnett and N. F. Scherer, *IEEE J. Sel. Top. Quantum Electron.*, 1998, **4**, 353–359.
24 M. C. Beard, G. M. Turner and C. A. Schmuttenmaer, *J. Phys. Chem. B*, 2002, **106**, 7146–7159.
25 S. Park, B. N. Flanders, X. Shang, R. A. Westervelt, J. Kim and N. F. Scherer, *J. Chem. Phys.*, 2003, **118**, 3917–3920.
26 D. F. Underwood and D. A. Blank, *J. Phys. Chem. A*, 2003, **107**, 956–961.
27 A. M. Moran, S. Park and N. F. Scherer, *Chem. Phys.*, 2007, **341**, 344–356.
28 J. A. Gardecki, M. L. Horng, A. Papazyan and M. Maroncelli, *J. Mol. Liq.*, 1995, **65/66**, 49–57.
29 A. J. Ruggiero, N. F. Scherer, G. M. Mitchell, G. R. Fleming and J. N. Hogan, *J. Opt. Soc. Am. B*, 1991, **8**, 2061–2067.
30 T. B. Norris, *Opt. Lett.*, 1992, **17**, 1009–1011.
31 Y.-H. Liau, A. N. Unterreiner, D. C. Arnett and N. F. Scherer, *Appl. Opt.*, 1999, **38**, 7386–7391.
32 A. A. Maznev and K. A. Nelson, *Opt. Lett.*, 1998, **23**, 1319–1321.
33 G. D. Goodno, V. Astinov and R. J. Dwayne Miller, *J. Phys. Chem. B*, 1999, **103**, 603–607.
34 M. Khalil, N. Demirdoven, O. Golonzka, C. J. Fecko and A. Tokmakoff, *J. Phys. Chem. A*, 2000, **104**, 5711–5715.
35 Q.-h. Xu, Y.-Z. Ma and G. R. Fleming, *Chem. Phys. Lett.*, 2001, **338**, 254–262.
36 M. Khalil, O. Golonzka, N. Demirdoven, C. J. Fecko and A. Tokmakoff, *Chem. Phys. Lett.*, 2000, **321**, 231–237.
37 C. J. Fecko, J. D. Evaes and A. Tokmakoff, *J. Chem. Phys.*, 2002, **117**, 1139–1154.
38 I. A. Heisler and S. R. Meech, *J. Chem. Phys.*, 2010, **132**, 174503.
39 A. Tokmakoff, *J. Chem. Phys.*, 1996, **105**, 1–11.
40 S. Mukamel, *Principles of Nonlinear Optical Spectroscopy*, Oxford University Press, New York, 1995.
41 R. M. Stratt, *Acc. Chem. Res.*, 1995, **28**, 201.
42 B. M. Ladanyi and R. M. Stratt, *J. Phys. Chem.*, 1995, **99**, 2502–2511.
43 B. M. Ladanyi and R. M. Stratt, *J. Phys. Chem.*, 1996, **100**, 1266.